CREATING VIRTUALLY DISTORTION-FREE MULTI-BAND FRAME IMAGES: LABORATORY AND FLIGHT CALIBRATION TECHNIQUES FOR THE LEICA RCD30

U. Tempelmann [a] , U. Beisl [a] , N. Boehrer [a] , L. Hinsken [b] , U. Recke [a]

[a] Leica Geosystems AG, Heerbrugg, Switzerland, Udo.Tempelmann@leica-geosystems.com
[b] Program Author of ORIMA, Germany, Ludger.Hinsken@LH-Ing.de

KEY WORDS: Calibration, Bundle Adjustment, RCD30

ABSTRACT:

The RCD30 is a four-band (RGB and NIR) medium format camera consisting of a single lens and two frame sensors behind a dichroic beam splitter. Therefore the light travels on different optical paths until it reaches the frame sensors. In order to get a distortion free four-band image, the position of each pixel in each image (RGB and NIR) needs to be corrected using pre-defined parameters. This paper describes the geometric calibration process for the RCD30 frame sensor. The calibration process relies on correction grids that can be obtained either from a bundle adjustment calculation with calibration flight images or from direct measurements done in the laboratory using a high precision goniometer. For the first method, the new implementation of the bundle adjustment software ORIMA is used. The calculation of the correction grid within the overall adjustment process is described in more detail. As a second method, a laboratory calibration process was established to avoid the costs of a calibration flight for every single camera. A comparison will show that both procedures deliver comparable calibration results. The correction grids produced by the calibration are fed into the new post-processing software called Leica FramePro, which then delivers distortion-free multi-band images. Those rectified images can then be further processed on any digital workstation without having to handle camera specific parameters.

1. INTRODUCTION

Color-RGB and False-color-Infrared (FCIR) images have long been used in aerial photography. However, until recently, medium format cameras were only allowing the acquisition of one of the two image types at a time. Placing a blue-blocking filter instead of a NIR-blocking filter in front of the lens system, the sensitivity of the blue CCD cells for NIR can be used to capture a relatively poor quality FCIR image. The medium format camera Leica RCD30 can deliver a co-registered four-band (RGB and high spectral quality NIR) image in a single exposure using a single lens and two frame sensors behind a dichroic beam splitter.

The beam splitter causes small non-radial-symmetric distortions in the NIR image. This suggests using a correction grid instead of a standard parametric distortion model.

This paper describes two ways to calibrate the RCD30. The first way is based on a bundle adjustment calculation with an image block from a dedicated calibration flight whereas the second way is based on a laboratory calibration with specially designed equipment and software. Both ways lead to the same set of calibration parameters. The laboratory process has the advantage of being more cost-efficient compared to a dedicated flight and being independent from weather conditions. This makes it the preferred way for the initial factory calibration. The calibration by bundle adjustment calculation from a test flight image block is the preferred method for camera re-calibration. It can be performed anywhere in the world and does not require shipping the camera to a calibration laboratory.

If the sensor is equipped with an IMU system, the misalignment must be calibrated with a calibration flight. This paper focuses on the RCD30 frame sensor calibration - the misalignment calibration is beyond the scope of this paper. The interested reader can refer to (Hinsken, 2002) for a detailed description of misalignment calibration.

The RCD30 has interchangeable lenses with a mount that ensures accurate repositioning of the lens on the camera body. The calibration approach has been driven by the design of the camera, requiring two frame sensors with different light paths. This design leads to a band specific calibration that allows for generating geometrically distortion free four-band images.

To illustrate the effect on the imagery, Figure 1 shows magnified small patches from the top right corner of an RCD30 image in raw form and with the calibration applied. In RGB we see that color fringes that result from chromatic aberration in the lens system are removed. In FCIR we see that also the large offset between RGB and NIR can be handled properly.

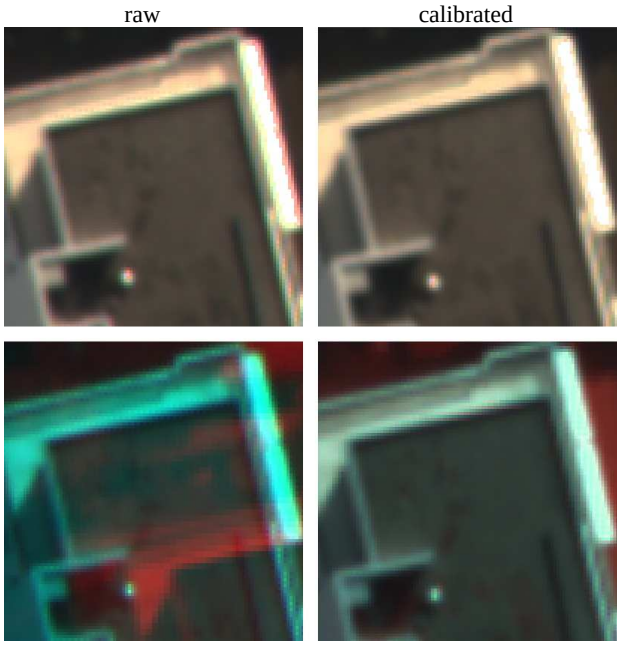

Figure 1. A raw and geometrically calibrated image patch in RGB (top) and FCIR (bottom)

2. DESIGN ASPECTS OF THE RCD30

The RCD30 design focused on creating a compact four-band camera head with good geometric stability, and at a reasonable cost level. Figure 2 shows a sectional view of the sensor head.

The elements having the biggest impact on the price of the camera head are the lens system and the CCD sensors. In order to keep the costs low, the decision has been made to re-use and adapt existing studio photography components. However, special care has been taken to ensure that those elements are suited for photogrammetric applications. The need for a stable geometry and focus over the wide temperature range of a flight led to a new rigid and a-thermalized lens system housing. A special mount makes sure that the lens system is re-positioned within 2 µm after exchange. The sensors are two (almost) off-the-shelf 60 megapixel CCD chips. The NIR CCD does not have a Bayer filter and is used in the 2x2 digitally binned mode. This increases the sensitivity and eliminates odd-even effects originating from spectrally adapted sensitivities in the original Bayer cells of the RGGB version.

The spectral separation between RGB and NIR is done by a dichroic beam splitter plate that reflects RGB at 90° and lets NIR pass straight through. The RGB light is reflected on the planar surface of the beam splitter and is only affected by radial symmetric distortion caused by the lens system. In the NIR light path, the light has to pass through the beam splitter plate, which behaves in non parallel light at 45° inclination angle like an aspheric element. The sharpness of the NIR image is ensured by a dedicated aspherical surface on the rear side of the beam splitter plate. Figure 9 shows a practical example of the NIR distortion.

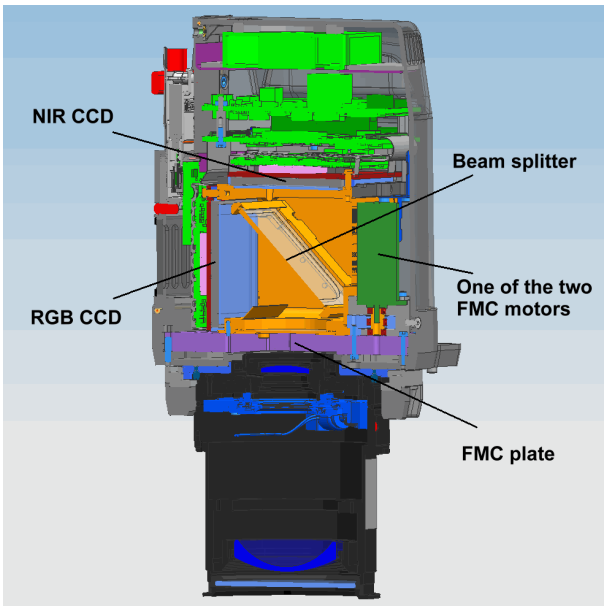

Figure 2. Mechanical and optical core of the RCD 30

The Bayer pattern does not allow the use of the Time Delay Integration (TDI) for Forward Motion Compensation (FMC) on the chip itself. Therefore a motorized FMC had to be designed. It shifts the whole focal plate unit consisting of the beam splitter, both CCDs and the front-end electronics. This concept has the following advantage over TDI: Combining two orthogonal drives allows proper operation also for large drift angles.
The FMC position in both axes is measured continuously to sub-µm accuracy, and the mid-exposure positions are stored with each image. Thus the image registration can be corrected for FMC movements.

3. CALIBRATION APPROACHES

The calibration and the co-registration of the spectral bands are handled separately. The green band was chosen as the geometric reference because it has two advantages over the other Bayer bands: the sampling is 2 times denser, and the design of the optical elements is optimized for this spectral range. In order to correct for the chromatic aberrations and ensure co-registration, the calibration provides corrections for each band independently.

For the laboratory calibration the camera is modeled as a five-band system, using the original 15 megapixel images for each of the Bayer cell elements - Red, Green1, Green2, Blue - and the 15 megapixel image for the binned NIR. Green1 is used as the reference for aligning the calibration device. In a second step the distortions are measured for each band using 5-band images of pinholes, laid out in a regular grid centered at the principal point for the Green1 image.

The calibration by bundle adjustment relies on images created by Leica FramePro (Chapter 5). These are four single band images (Red, Green, Blue and NIR) interpolated to the full sensor resolution of 60 megapixel. Either a previous laboratory or flight calibration or just nominal values are used as a first approximation.

The results of both calibrations are modeled in vector fields of corrections for each band. The distortions are calculated using a nominal focal length of 53 (resp. 83) mm instead of the real paraxial focal lengths of about 51.7 (resp. 81.0) mm for the 50 (resp. 80) mm lens systems. The up-scaling of the focal length of about 2.5% makes sure that the rectified four-band images have the original pixel count without containing any black margins caused by distortion effects or a de-centered principal point coming from chip mounting tolerances.

The distortion correction fields are saved into an XML file that contains a regular grid of corrections for each of the four bands. The grids are covering a slightly bigger area than the real image and are sampled dense enough to allow for using bi-linear interpolation in the rectification.

The laboratory calibration process cannot determine the IMU misalignment estimation (exterior orientation). Furthermore, usually the IMU sensor is delivered separately from the sensor head. Thus the principal point offset has to be determined based on flight images taken with an assembled system. This can easily be done by the customer himself using IPAS-CO+ whenever IMU and sensor head had to be separated.

4. LABORATORY CALIBRATION

The laboratory setup consists of a collimator projecting selectable pinhole images to infinity and a 2-axis goniometer that rotates the camera head such that the pinhole images can be viewed at any direction within the field of view (FOV) of the camera lens (Figure 3). Both units have been especially designed for the RCD30.

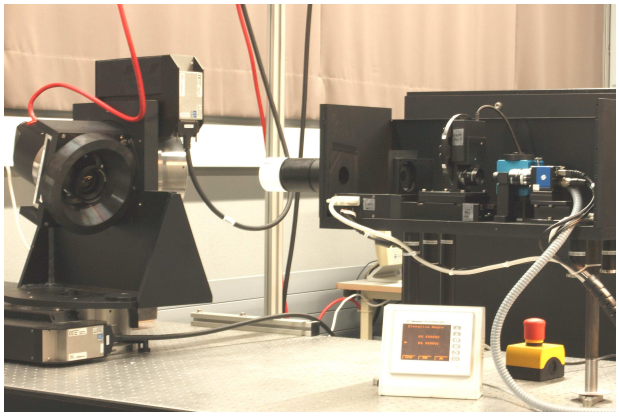

Figure 3. The goniometer and collimator setup, baffles and lids removed

The goniometer is based on two large high-precision rotation stages (absolute accuracy 0.003°) in azimuth-elevation configuration similar to a theodolite. This allows for "transiting the scope" (measuring in direct and reverse position) by flipping over both goniometer axis to measure with the sensor image being upside down (i.e. turning the elevation axis by 180° and the azimuth axis by 180°-2*azimuth angle). Averaging the two measurements eliminates most of the residual non-orthogonality of the two axes and compensates for internal deformations of the camera caused by the horizontal operating position.

The collimator system is not only used for the geometric calibration, but also for the sharpness adjustment of the camera. Besides that, it allows to check the camera resolution. The elements necessary to cover all tasks are

- A collimation lens (a small ED-apochromatic astronomic telescope lens f = 339 mm, D = 45mm).
- A small integrating sphere for the illumination of the projection patterns.
- A beam splitter cube that splits the light path for illumination and autocollimation.
- A frame camera for autocollimation (adjustment of the infinity position).
- A high precision rotation stage (unidirectional repeatability 0.0007°) that allows exchanging the projected patterns (pinholes, barcodes etc.) in a very repeatable way.
- A linear stage that allows controlled (de-)focusing of the projected pattern for focus adjustment. For geometric calibration the stage is in the infinity position.

In order to maintain a long-term stability the geometric calibration unit has been set up in a temperature controlled room. The calibration of the rotation stages has been verified with a calibrated polygon mirror. The orthogonality of the two goniometer axes is better than 0.005°.
Angular and focus calibration are checked on a regular basis. Up to now, no change could be detected. That means that individual calibrations per measurement are not necessary.

The projection patterns used are:

- Pinhole (1 mm diameter) for geometric calibration.
- Coarse bar codes for focus adjustment (1 lp/mm, horizontal and vertical), including the infinity reference by autocollimation.
- Bar codes for MTF measurement at the lens systems supplier's specification level of 20 lp/mm at 50 and 80 mm focal length (3 lp/mm and 5 lp/mm, horizontal and vertical).
- Crosshair pattern for angular zero adjustment and orthogonality check.

The point measurement is done using a pinhole that is collimated to infinity. This pinhole is imaged to an ellipse of about 25 (resp. 40) pixels diameter on the CCDs for the 50 (resp. 80) mm lens. Using the known approximate imaging parameters, a template image is created that is sub-pixel-correlated to the pinhole image in all five 15 megapixel images of the camera head. Due to the larger amount of correlation calculations a larger object can be matched to higher precision than a smaller object.

For practical reasons the definition of the distortion of analog airborne imaging cameras was defined following the measurement procedure at that time (Kraus, 1986, p. 29): Instead of the film, a highly precise glass plate with equidistant grid lines across the image diagonals was placed in the image plane of the camera lens. The angles under which the grid points were observed on the object side of the lens were measured with a goniometer (McGlone, 2004, sec. 8.5.2.2). Using the paraxial focal length and a pinhole camera model the undistorted positions could be projected into the image plane.
Then the distortion was defined as the difference of the distorted (equidistant grid) position minus the undistorted (projected) position measured at the distorted (equidistant grid) position. This definition is still used in all bundle adjustment software, including ORIMA, and also in the RCD30 post-processing software Leica FramePro.
Unfortunately in modern digital cameras a grid plate cannot replace the focal plate without invalidating the focal adjustment and principal point calibration.
So the distortion for digital cameras has to be measured the other way round: A pinhole image is projected at precisely calculated multiple angular positions into the image plane of the camera. The angular grid corresponds to an equidistant object grid. With the assumed nominal focal length and a pinhole camera model the undistorted positions can be projected into the image plane and be compared with the observed distorted point positions, which form a non-equidistant grid. Calculating the distortion as above will end up in a distortion grid at non-equidistant grid points.

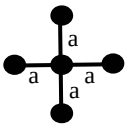

Figure 4. Sensor rotation and principal point measurement pattern

Therefore the geometric distortion measurement is done in three steps.

1. The sensor rotation and the principal point position are determined by measuring the five characteristic points of an equidistant cross in the Green1 reference band (Figure 4). The result is refined in 5 iterations.
2. According to the sensor rotation and the principal point position an equidistant grid of 11x13 points (Figure 5) is laid out in the object (=angle) space and the distorted points are measured in the image plane

in direct and reverse position of the sensor head. The non-equidistant distortion grid is interpolated to equidistant grid positions. For the outmost points this is even a short distance extrapolation.

3. Based on the interpolated grid that results from step 2, the modified goniometer angles are calculated. The measurement is repeated in direct and reverse position of the sensor head and the observed distorted points will fit almost exactly to an equidistant grid in the image plane. Then the final distortion grid is calculated and interpolated again.

As the Leica FramePro software expects a grid that is larger than the image, an additional line of points is added, using an extrapolation model that was empirically derived from flight calibrations.

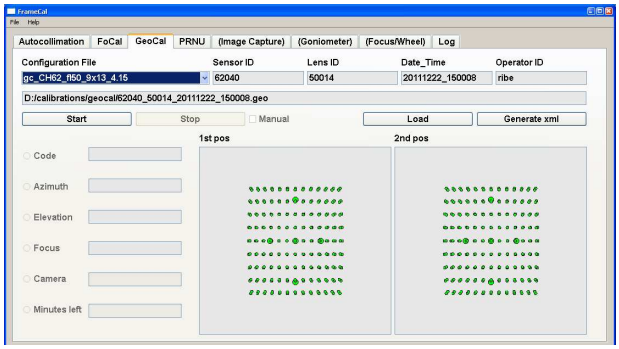

Figure 5. Measurement grid in direct and reverse position. The five larger dots show the positions of the rotation and principal point measurement.

5. IMAGE RECTIFICATION IN LEICA FRAMEPRO

Leica FramePro rectifies the raw images to distortion free multi-band images with a nominal principal distance, using an equidistant grid of distortion corrections, read from the calibration XML file. In addition, a principal point offset correction that is also contained in the XML file and the mid-exposure FMC-position from the image header are applied.

A main design goal was to use a simple data model that can be easily integrated into in-house and third party software packages. It was important to choose a suitable distortion parameter format, such as ASCII text files containing Australis Parameters, the pat-b output format, or the ORIMA-Camera-File (DC-Brown parameters). A decision for any of these formats would have meant to provide converters for all the other formats. Otherwise users would try their own error prone conversions and introduce conversion errors.

Additionally we would have had to handle at least 2 different calibration sets. One set would describe the RGB image, the other the NIR image from the second sensor. This would add additional complexity for the data handling to the customer.

On the other hand, since the RGB data originates from a Bayer sensor, a data interpolation is already needed.

So it became the obvious choice to combine Bayer interpolation and distortion correction in a single interpolation process, which avoids exporting any distortion parameters. This also gives the advantage of a very simple geometric description by a plain pinhole camera model with a nominal principal distance. Furthermore, precisely co-registered four-band, RGB or FCIR images can be more easily processed by subsequent software packages than separate images with different geometries.

Leica FramePro is mainly designed for image download, simple post flight quality control and creation of image files tailored to different customer needs. To do this efficiently, the notion of a processing chain is used. This chain can be thought of as a simple control mechanism that is able to run multiple kernels sequentially. Each kernel itself is specialized in one task and runs data parallel. The data flow follows a bucket chain pattern passing data from kernel to kernel.

Goals for the rectification algorithm were especially

- grid based interior orientation (distortion correction)
- very good throughput on reasonably CPUs
- no requirement of additional hardware (however, Leica FramePro requires at least 8 GB of RAM and a 64 bit Windows operating system)

Parallelization relies on OpenMP as it can run freely (without thread synchronization), as

- the algorithm uses indirect interpolation (for each target pixel we calculate the exact position in source image space and interpolate the intensity there), which enables atomic writes per pixel
- the grid is slightly bigger than the full sensor space (simple look-up and interpolation)
- all parameters that may vary are integrated into the distortion correction grid beforehand (these are a modified principal point and the mid-exposure position of the FMC)

All processing is done in real value precision avoiding quantization (rounding) errors. In the current Leica FramePro version (1.1) we still do de-mosaicking and rectification in separate kernels. In future it is planned to get better quality by joining these two steps for the RGB sensor avoiding one resampling step.

6. EXTENDED BUNDLE ADJUSTMENT

With a special flight configuration, known as the double cross (Figure 6), which was already established for calibration of the ADS line sensor, it is possible to fully calibrate frame sensors, too. The configuration is characterized by a cross shape, where each line is flown bi-directionally. Two such crosses are required at different flying heights. The double cross is flown with about 70 % overlap in each flight direction, which results in a maximum of 24 ray points. The second flying height is about 30 % above the first flying height.

Using this configuration allows for a calibration without using ground control points. The GPS-IMU observations done at two different flying heights define the scale and allow for performing a calibration over flat terrain. The flight configuration was designed in such a way that it reduces the correlation among the camera parameters to a minimum. It also has the advantage of reducing the correlation between the camera and the exterior orientation parameters and ensures that the calibration isn't influenced by the flight configuration.

The algorithm used for automatic point measuring must be able to handle large scale differences and a high number of rays per point. The software used to perform this task is either “LPS Automatic Tie Point Extraction” or “IPAS CO+ APM”.

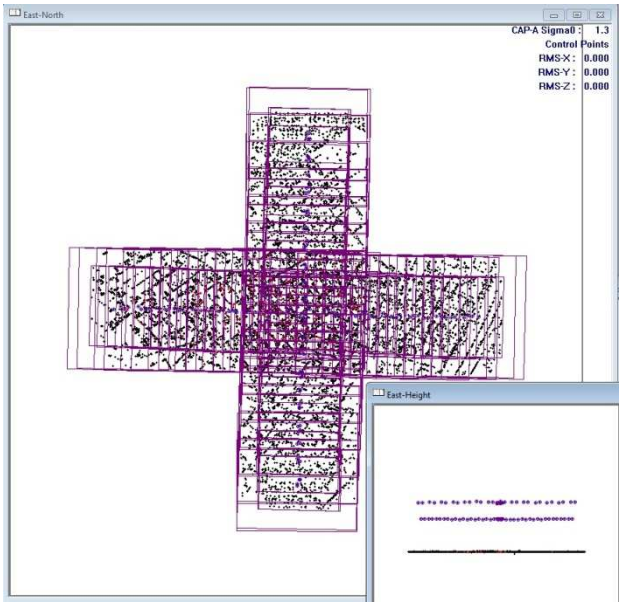

Figure 6. Double cross flight configuration

The mathematical model of the bundle adjustment algorithm is based on the transformation of a 3D point from ground space into the 2D image space.

$$\begin{bmatrix} x_{ij} \\ y_{ij} \\ -f \end{bmatrix} = \lambda_{ij} \mathbf{R}(\omega,\varphi,\kappa)_j \begin{bmatrix} X_i - X_j \\ Y_i - Y_j \\ Z_i - Z_j \end{bmatrix} \quad (1)$$

$\begin{bmatrix} X_i \\ Y_i \\ Z_i \end{bmatrix}$ Coordinates of object point

$\begin{bmatrix} X_j \\ Y_j \\ Z_j \end{bmatrix}$ Coordinates of projection center

$\mathbf{R}(\omega,\varphi,\kappa)_j$ Rotation between object and image coordinate system

$\begin{bmatrix} x_{ij} \\ y_{ij} \\ -f \end{bmatrix}$ Image coordinates and principal distance

By dividing equations one and two by equation three in (1) above, the unknown scale λ_{ij} cancels out. These equations are the collinearity equations as used for frame sensors.

$$x_{ij} = -f \frac{r_{11_j}(X_i - X_j) + r_{12_j}(Y_i - Y_j) + r_{13_j}(Z_i - Z_j)}{r_{31_j}(X_i - X_j) + r_{32_j}(Y_i - Y_j) + r_{33_j}(Z_i - Z_j)} \quad (3)$$

$$y_{ij} = -f \frac{r_{21_j}(X_i - X_j) + r_{22_j}(Y_i - Y_j) + r_{23_j}(Z_i - Z_j)}{r_{31_j}(X_i - X_j) + r_{32_j}(Y_i - Y_j) + r_{33_j}(Z_i - Z_j)} \quad (4)$$

This model describes a ray that travels on a straight line from the object through the projection center to the image. It must be extended to describe the physical effects that happen when the ray passes through the lens and other camera components until it reaches the sensor surface.

$$x_{ij} = -f \frac{r_{11_j}(X_i - X_j) + r_{12_j}(Y_i - Y_j) + r_{13_j}(Z_i - Z_j)}{r_{31_j}(X_i - X_j) + r_{32_j}(Y_i - Y_j) + r_{33_j}(Z_i - Z_j)} + dx \quad (5)$$

$$y_{ij} = -f \frac{r_{21_j}(X_i - X_j) + r_{22_j}(Y_i - Y_j) + r_{23_j}(Z_i - Z_j)}{r_{31_j}(X_i - X_j) + r_{32_j}(Y_i - Y_j) + r_{33_j}(Z_i - Z_j)} + dy \quad (6)$$

The terms *dx* and *dy* can be defined in various ways. In ORIMA the well-known parameter set of (Brown, 1976) is used.

$$\begin{aligned} dx = {} & x_0 + a_1(r^2 - r_0^2)x + a_2(r^4 - r_0^4)x + a_3(r^6 - r_0^6)x \\ & + b_1 x + b_2 y \\ & + (c_1(x^2 - y^2) + c_2 x^2 y^2 + c_3(x^4 - y^4))x / c \\ & + d_1 xy + d_2 y^2 + d_3 x^2 y + d_4 xy^2 + d_5 x^2 y^2 \end{aligned} \quad (7)$$

$$\begin{aligned} dy = {} & y_0 + a_1(r^2 - r_0^2)y + a_2(r^4 - r_0^4)y + a_3(r^6 - r_0^6)y \\ & + (c_1(x^2 - y^2) + c_2 x^2 y^2 + c_3(x^4 - y^4))y / c \\ & + d_6 xy + d_7 x^2 + d_8 x^2 y + d_9 xy^2 + d_{10} x^2 y^2 \end{aligned} \quad (8)$$

For the RCD30 calibration only the coordinates of the principal point x_0, y_0 and the radial lens distortion parameters $a_1 ... a_3$ are used. The remaining parameters are not suitable to compensate the systematic effects of the sensor.

The vectors at the grid points (e.g. in Figure 9) are calculated as mean values of the residuals of the nearest neighbor points. If the residuals would have no systematic, the average values would be zero.
Extending the corrections can compensate these regional effects.

$$x_{ij} = -f \frac{r_{11_j}(X_i - X_j) + r_{12_j}(Y_i - Y_j) + r_{13_j}(Z_i - Z_j)}{r_{31_j}(X_i - X_j) + r_{32_j}(Y_i - Y_j) + r_{33_j}(Z_i - Z_j)} + dx + \overline{dx} \quad (9)$$

$$y_{ij} = -f \frac{r_{21_j}(X_i - X_j) + r_{22_j}(Y_i - Y_j) + r_{23_j}(Z_i - Z_j)}{r_{31_j}(X_i - X_j) + r_{32_j}(Y_i - Y_j) + r_{33_j}(Z_i - Z_j)} + dy + \overline{dy} \quad (10)$$

$$\begin{aligned} \overline{dx} = {} & cx(i,j)(1-\Delta x)(1-\Delta y) + cx(i+1,j)\Delta x(1-\Delta y) \\ & + cx(i,j+1)(1-\Delta x)\Delta y + cx(i+1,j+1)\Delta x \Delta y \end{aligned} \quad (11)$$

$$\begin{aligned} \overline{dy} = {} & cy(i,j)(1-\Delta x)(1-\Delta y) + cy(i+1,j)\Delta x(1-\Delta y) \\ & + cy(i,j+1)(1-\Delta x)\Delta y + cy(i+1,j+1)\Delta x \Delta y \end{aligned} \quad (12)$$

cx(i,j), cy(i,j) : Corrections at grid point (i,j)

$$\Delta x = \frac{x - gx(i,j)}{d}$$

$$\Delta y = \frac{y - gy(i,j)}{d}$$

with: *gx(i,j)* = x-coordinate at grid point (i,j)

with: *d* = mesh-size

The equations 11 and 12 describe a bilinear interpolation within a mesh of a grid. The corners of each mesh are given by the predefined fixed grid coordinates *gx(i,j)* and *gy(i,j)*. The size of a mesh has to be chosen in such a way that the local systematic can be compensated by linear interpolation.
The corrections *cx(i,j)* and *cy(i,j)* are introduced as unknown parameters in the bundle adjustment. The number of parameters depends on the mesh-size and the image format. Typically there are a few hundred of correction parameters. In the case of the RCD30 a mesh-size of 4.15 mm leads to (13·15·2) = 390 parameters. The automatic point measurement provides more than 200 image points for estimating each correction parameter (Figure 7).

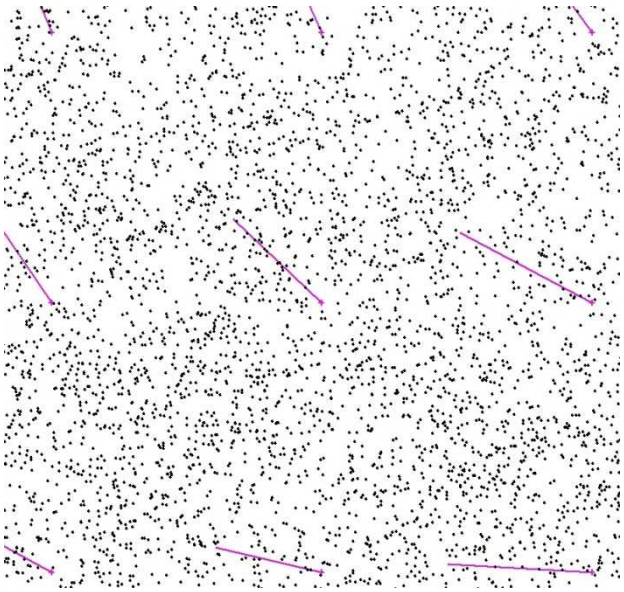

Figure 7. Illustration of the point density used to determine the correction grid parameters. The figure shows a zoomed portion of the image, showing four meshes.

The correction grid model can be applied to any type of frame sensor. It can be used for instance for other frame sensors like DMC, UltraCam or DigiCam by adapting the size of the grid and the size of the meshes.

Integrating the grid parameter estimation into the bundle adjustment, instead of estimating the grid coefficients from the remaining residuals after the bundle adjustment, has the advantage that the solution is more rigorous and the result is obtained faster. Uncompensated systematic in an adjustment can cause various side effects like small blunders remaining undetected or good observations being erroneously detected as blunders, other parameters being biased, or weights being impacted within the variance component estimation.
The bundle adjustment, which takes longer when grid parameters are used, is still faster than if the grid parameters were estimated in an iterative post-process. The integrated process is a more rigorous approach as it relies on the original observations, whereas post-process-corrected observations would have to go into an iteration process and assume uncorrelated observations which isn't fully true.

7. THE CALIBRATION PROCESS BASED ON BUNDLE ADJUSTMENT

The design of the RCD30 using an aspherical beam splitter plate for the NIR band is a highly non-linear system that requires an iterative process for the calibration. Each iteration step consists of automatic tie-point measurements followed by a bundle adjustment, which solves sets of calibration parameters. Those calibration parameters are then used to update the correction grids, which are then used to generate a new set of rectified images. This iterative process is continued until all bands are co-registered and are free from geometrical distortions. Depending on the magnitude of the IMU misalignment and the relative shift and rotation of the NIR sensor against the RGB sensor, the calibration needs four to six iterations.

The iterative process starts with the green band only. A relatively sparse set of points is extracted by an APM run with a strategy that allows for large offsets. The result is used to solve in the bundle adjustment for IMU misalignment, principal point, principal distance and radial-symmetric distortion (Figure 8). After applying the green band results to all bands, a second iteration is started, now with a very dense point extraction by APM (Figure 7). The bundle adjustment is used in grid mode to solve for small effects, such as irregular deformations from non-planarity of the CCD.

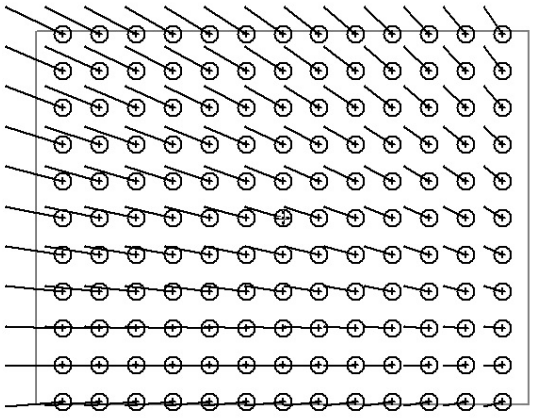

Figure 8. Effect of the principal distance and the principal point during the first iteration. The circles serve as scale indicators and have a radius of 10 µm.

In a second phase all bands are included into the process. If it turns out during the first iteration of this phase that the misalignment calculated from the green band is not yet stable, the iteration is used as a third green-only iteration.

The second phase consists of two or three iterations plus a final check. In the first iteration of the second phase, the NIR image is introduced for the first time. The specificity of the camera design regarding the NIR imagery (the independent sensor and a light path with more optical elements than the RGB path) will lead to an important offset and distortions pattern after the first iteration in that second phase (Figure 9).

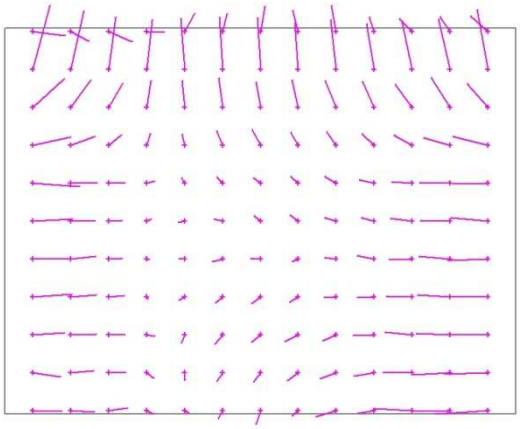

Figure 9. Systematics compensated in the first iteration for the NIR band. The maximum values reach 12 µm.

During the second phase, the bundle adjustment is used in grid mode for each band individually. To increase the convergence speed of the process, D.C. Brown parameters are used additionally to compensate for the larger deformations in the first NIR iteration. After a total of four or five iterations the remaining systematic is reduced to about 0.1 µm (Figure 10).

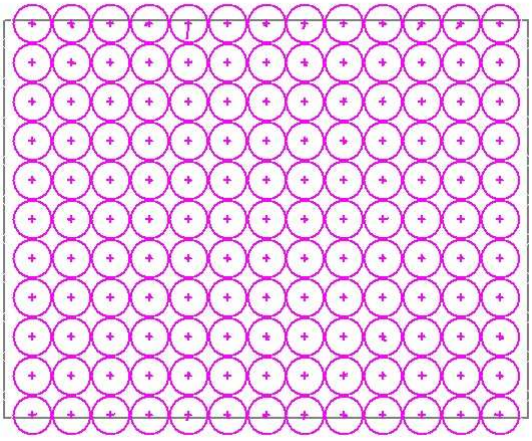

Figure 10. Remaining systematics for the NIR band at the grid points, when grid estimation is used. The diameter of each circle is 1 µm. The results for the RGB bands look similar.

However, besides the internal accuracy of the bundle adjustment, there is also the external accuracy of an iteration step. Due to the point location errors in APM, appending another iteration step will always show new random effects, smaller than 1 µm across for most of the image, up to 2 µm on the border points and sometimes larger on the corner points (Figure 11). The larger values at the border and the corners are due to the small number of tie points generated in this region. As they affect only the outmost image region, they can be neglected.

A final quality control is done ensuring that the estimated calibration parameters are delivering a distortion free image. No noticeable color fringes should appear in the RGB and FCIR images.

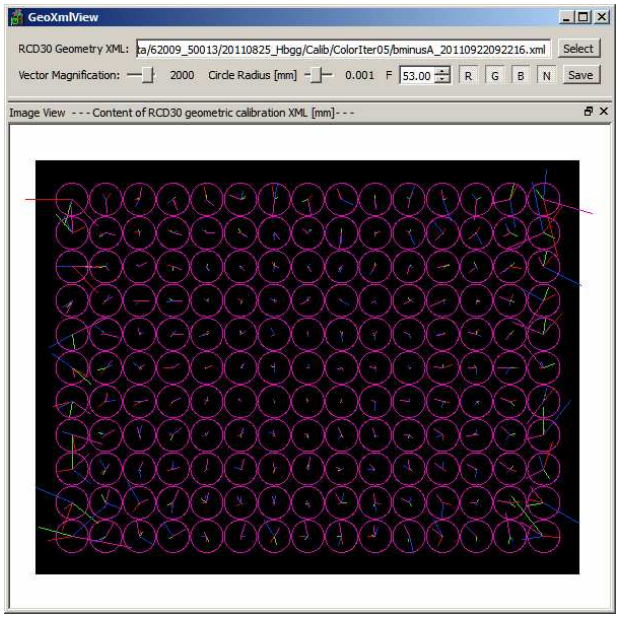

Figure 11. Remaining variation of the correction grid from an additional iteration. The result is typical, regarding the size of the variation. There is no further convergence of the solution.

8. COMPARISON OF THE RESULTS OF BOTH CALIBRATION METHODS

As the flight-based calibration will always compensate a part of the IMU misalignment in the correction grid, the results of both methods cannot match directly. The best way to compare both methods is to run a single bundle adjustment iteration with a goniometer calibration as the input. The bundle must be used to estimate only the two parameters IMU misalignment and principal point. This is the same as a customer has to do when he receives a goniometric calibration. The image space residuals of this bundle adjustment show how much the goniometric calibration differs from what would result from the flight.
A typical result of such a comparison is shown in Figure 12.

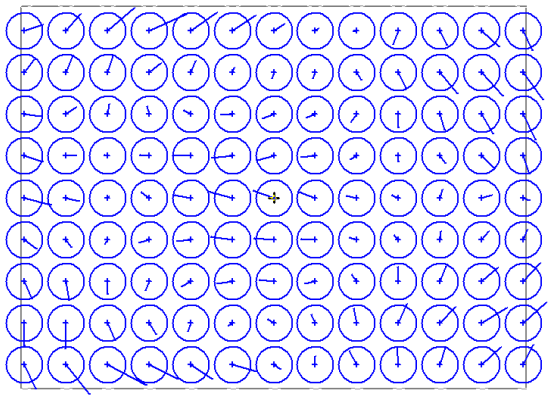

Figure 12. Difference of goniometric and flight-based distortion corrections. The diameter of each circle is 4 µm.

There is clearly some systematics visible. These are however smaller than 2.5 µm except for the top and bottom edge, where the maximum value is 5 µm. The resulting σ_0 is 2.1 µm.

Keeping in mind, that this is a Bayer camera with a Bayer cell size of 12 µm, the result is still good.

9. CONCLUSION

The flight based calibration method, using a combination of classical camera parameters and the new grid point estimation of ORIMA has been proven to work well for the RCD30, even with its uncommonly shifted, rotated and distorted NIR band. Therefore we expect it to work also for other frame cameras. Currently we are running tests with the Z/I DMC II 250, which has the additional challenge of containing local deformations on the huge CCD area. Other cameras will be considered for grid correction as well.

Getting the goniometric calibration to a sufficient quality level was a non-trivial and tedious task, both on the hardware and the software side. Although the current agreement of the goniometer and the bundle adjustment results is sufficient for practical purposes, we will further investigate the small systematic effects which we see between both methods. As ORIMA has proven to deliver as perfect as possible results over quite some years, we will focus our search on the goniometer side.

REFERENCES

Brown, D.C., 1976. The Bundle Adjustment. Progress and Prospects. XIIIth Congress of the ISP, Com. III, Helsinki, Finland.

Hinsken, L. et al., 2002. Triangulation of LH Systems' ADS40 Imagery using ORIMA GPS/IMU. ISPRS Commision III Symposium, Graz, Austria.
http://www.isprs.org/proceedings/XXXIV/part3/papers/paper029.pdf

Kraus, K., 1986. Photogrammetrie (Band 1). Dümmler, Bonn, Germany.

McGlone, J.C., Mikhail, E.M., Bethel, J. (eds.), 2004. Manual of Photogrammetry (Fifth Edition). ASPRS, Bethesda, USA.